38th AIAA/ASME/SAE/ASEE Joint Propulsion Conference & Exhibit
7-10 July 2002, Indianapolis, Indiana

AIAA 2002-3974

AFRL MicroPPT Development for Small Spacecraft Propulsion

Gregory G. Spanjers, Daron R. Bromaghim, Capt. James Lake, Michael Dulligan
AFRL Propulsion Directorate, Edwards AFB, CA

David White, John H. Schilling, Stewart Bushman
W.E. Research, Rosamond, CA

Erik L. Antonsen
Rodney L. Burton
University of Illinois at Urbana–Champaign, IL

Michael Keidar
Iain D. Boyd
University of Michigan, Ann Arbor, MI

A class of miniaturized pulsed plasma thrusters (PPT), known as MicroPPTs,' is currently in development at the Air Force Research Laboratory. The MicroPPTs use a surface discharge across solid Teflon™ propellant to provide precise impulse bits in the 10 μN–s range. In the near term, these thrusters can provide propulsive attitude control on 150–kg–class spacecraft using 1/5th the *dry* mass of conventional torque rods and reaction wheels.' Eventually these thrusters are designed for primary and attitude control propulsion on future 25–kg class spacecraft. Efforts to characterize MicroPPT performance and the thruster plume are underway. To this end, a modified torsional thrust stand has been developed for the purpose of accurately measuring the low–level thrust generated by the MicroPPT. A Hemott Cell interferometer is introduced to establish the electron and neutral densities in the thruster plume. Comparison of the measured electron density with modeling predictions shows close agreement. Additionally, a Pockels cell has been developed to provide a zero–impedance MicroPPT breakdown voltage measurement, and an intensified CCD array has been used to characterize the divergence of both the thruster plume and the late–time particulate emission. A synopsis is also presented of the status of the thruster development, including lifetime, thermal, and environmental testing.

Introduction

The Air Force has a growing technological interest in highly maneuverable microsatellites to perform future missions such as space–based surveillance, on–orbit servicing, inspection, and space control. Eventually, these missions will be accomplished by fleets of 25-kg microsatellites operating independently or flying in formation to create sparse–aperture arrays. From a propulsion standpoint this mission requires spacecraft propulsion systems that can deliver high thrust (for rapid orbit transfers or close–proximity maneuvers), or high specific impulse (for stationkeeping, orbit maintenance, attitude control, or precision pointing and positioning).

One propulsion technology that the Air Force Research Laboratory has been developing in response to this requirement is the MicroPPT.' The MicroPPT is a miniaturized electric propulsion thruster that uses a pulsed electrical surface discharge across the face of solid Teflon™ propellant. The surface discharge ablates a portion of the solid Teflon™ propellant, ionizes it, and then accelerates it electromagnetically to generate thrust. The use of solid propellant eliminates the propellant feed system, since the propellant tanks and valves needed for liquid or gaseous propellant management are eliminated. The use of electromagnetic acceleration to create thrust leads to a high specific impulse compared to chemical propulsion systems. Major simplifications in the MicroPPT thruster design, as compared to the conventional PPT,[3] enable significant miniaturization of the device. Therefore the MicroPPT appears to be well–suited for the required high–specific impulse microsatellite propulsion applications.

This paper describes the current efforts for developing the AFRL MicroPPT. Testing completed to date is presented, along with a description of the tests to be completed. Discussion is also provided on some MicroPPT advances currently in progress in the laboratory.

Description of the APRL MicroPPT

A simple schematic of the MicroPPT is shown in Figure 1. A high voltage energy storage capacitor is connected directly to a coaxial propellant module. The propellant consists of a central conductive rod that serves as the cathode in the discharge. The cathode is surrounded by an annulus of Teflonm,

Report Documentation Page

Form Approved
OMB No. 0704-0188

1. REPORT DATE	2. REPORT TYPE	3. DATES COVERED
JUN 2002		**-**

4. TITLE AND SUBTITLE	5a. CONTRACT NUMBER
AFRL MicroPPT Development for Small Spacecraft Propulsion	5b. GRANT NUMBER
	5c. PROGRAM ELEMENT NUMBER

6. AUTHOR(S)	5d. PROJECT NUMBER
Gregory Spanjers; Daron Bromaghim; James Lake; Michael Dulligan; David White	**1011**
	5e. TASK NUMBER **0011**
	5f. WORK UNIT NUMBER

7. PERFORMING ORGANIZATION NAME(S) AND ADDRESS(ES)	8. PERFORMING ORGANIZATION REPORT NUMBER
Air Force Research Laboratory (AFMC),AFRL/PRSS,1 Ara Road,Edwards AFB,CA,93524-7013	

9. SPONSORING/MONITORING AGENCY NAME(S) AND ADDRESS(ES)	10. SPONSOR/MONITOR'S ACRONYM(S)
	11. SPONSOR/MONITOR'S REPORT NUMBER(S)

12. DISTRIBUTION/AVAILABILITY STATEMENT

Approved for public release; distribution unlimited

13. SUPPLEMENTARY NOTES

14. ABSTRACT

A class of miniaturized pulsed plasma thrusters (PPT), known as MicroPPTs, is currently in development at the Air Force Research Laboratory, Edwards Research Site, California. The MicroPPTs use a surface discharge across solid Teflon propellant to provide precise impulse bits in the 10 micro-newton-per-second range. In the near term, these thrusters can provide propulsive attitude control on 150-kg-class spacecraft using one-fifth the dry mass of conventional torque rods and reaction wheels. Eventually these thrusters are designed for primary and attitude control propulsion on future 25-kg class spacecraft. Efforts to characterize MicroPPT performance and the thruster plume are underway. To this end, a modified torsional thrust stand has been developed for the purpose of accurately measuring the low-level thrust generated by the MicroPPT. A Herriott Cell interferometer is introduced to establish the electron and neutral densities in the thruster plume. Comparison of the measured electron density with modeling predictions shows close agreement. Additionally, a Pockels cell has been developed to provide a zero-impedance MicroPPT breakdown voltage measurement, and an intensified CCD array has been used to characterize the divergence of both the thruster plume and the particulate emission. A synopsis is also presented of the status of the thruster development, including lifetime, thermal, and environmental testing.

15. SUBJECT TERMS

16. SECURITY CLASSIFICATION OF:			17. LIMITATION OF ABSTRACT	18. NUMBER OF PAGES	19a. NAME OF RESPONSIBLE PERSON
a. REPORT	b. ABSTRACT	c. THIS PAGE			
unclassified	**unclassified**	**unclassified**		**12**	

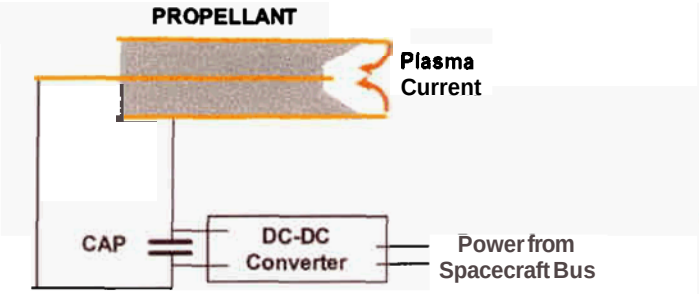

Figure 1: Simple MicroPPT schematic

which serves as the primary source of propellant. The Teflon™ propellant is then encased in a conductive tube, which serves as the anode. In the self-triggering configuration[4] shown in Figure 1, the DC-DC converter charges the capacitor to a high voltage. This voltage also appears at the electrodes and across the propellant face. At some point in the charge cycle, the electrode voltage exceeds the surface breakdown voltage of the propellant face, and the discharge self-initiates.

The surface discharge then ablates a small amount of the solid Teflonm material, ionizes it, and accelerates it from the thruster through primarily electromagnetic forces. The propellant has no traditional feed mechanism in this design. Over time the propellant and central electrode will recede back into the outer shell of the anode.

The general design philosophy for the AFRL MicroPPT has been to attempt fundamental changes in the PPT topology in order to accomplish significant reductions in the thruster dry mass. Compared to the benchmark LES 8/9 PPT,[3] the MicroPPT design eliminates the igniter sparkplug, trigger electronics, propellant housing structure, propellant spring, and one-half of the PPU. The result is a dry mass reduction between 10X and 20X over LES 8/9.

The major impediment to long-life operation of the MicroPPT is maintaining a clean propellant face. Experiments have shown that operation at insufficient E/A (where E is the discharge energy of a single pulse and A is the area of the Teflon™ propellant face) leads to the build up of a carbon layer on the propellant face.' This carbon layer ultimately causes thruster failure by shorting the electrodes.

Analysis has attributed this buildup to carbon neutrals returning to the propellant face at decreased propellant face temperatures.[6] The source of the neutrals is late-time vaporization observed to evolve

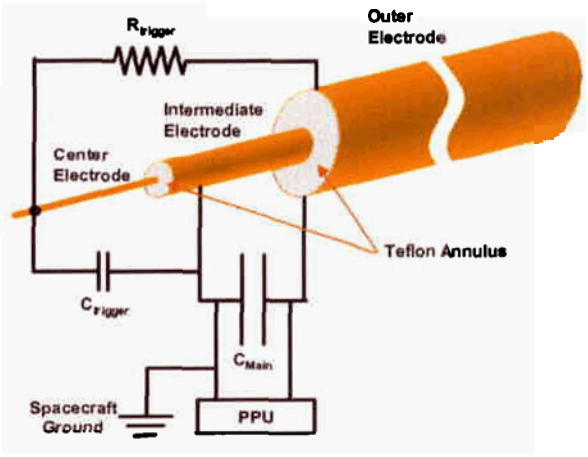

Figure 2: 3-Electrode MicroPPT configuration

from the PPT propellant face well after the current discharge has completed.[7] For a standard PPT this potential carbonization presents no major design issue. Since the discharge is actively triggered with a separately commanded circuit to a spark plug embedded in the cathode, all discharges are at the same fixed discharge energy, which is chosen to avoid carbonization of the propellant face. For the MicroPPT, which is self-triggered, shot-to-shot variations in the discharge energy can be significant. Although over extended timescales these variations average out and are expected to give a performance that scales with input power, a succession of low-energy discharges can lead to carbonization and eventual thruster failure. Previous work has characterized the operational parameters needed to achieve long-term MicroPPT operation without carbonization for relatively small diameter propellant.[5] Characterization and plume diagnostics at larger diameters are shown later in this paper.

Three-Electrode Design

The latest MicroPPT iteration uses a 3-electrode configuration' as shown in Figure 2. A small-diameter conductive rod is used as a "center electrode" and is surrounded by a small diameter annulus of Teflon™ propellant. This assembly is then encased in a conductive tube that acts as an "intermediate electrode." The intermediate electrode is surrounded by a second, larger, annulus of Teflon™, which is encased in a larger diameter outer conductive rod that acts as the "outer electrode."

The MicroPPT is fired by a low-energy breakdown between the intermediate and central electrode. This discharge provides enough seed ionization to enable the higher energy conduction breakdown between the intermediate and outer electrode. The discharge

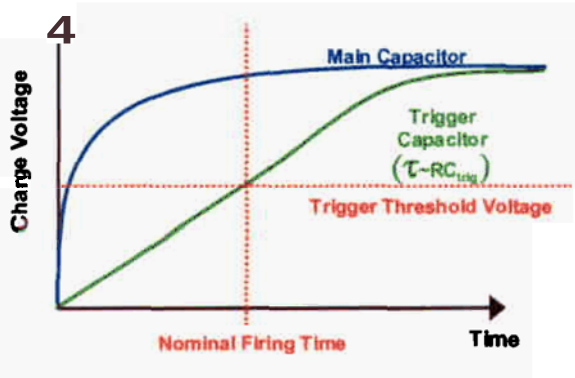

Figure 3: Energizing the 3–electrode MicroPPT capacitors

between the intermediate and central electrode is referred to as the "trigger discharge." The discharge between the intermediate and outer electrode is referred to as the "main discharge." Typically the trigger discharge energy is about 1/50th that of the main discharge.

The 3–electrode design is energized using the electrical circuit of Figure 2. When the PPU is commanded on, the circuit is designed to energize the capacitors as shown in Figure 3. The main capacitor quickly charges to the full output voltage of the PPU. The charge voltage on the main capacitor is designed to be well below the threshold for surface discharge initiation between the intermediate and outer electrode so discharge initiation is precluded. The charging rate of the trigger capacitor is greatly slowed by the large resistance in the charge path. Nominally, when the trigger capacitor reaches its threshold voltage for surface breakdown a discharge arc between the center and intermediate electrode will initiate. This small low–energy discharge will provide sufficient seed ionization near the propellant face that the main discharge will be initiated.

Using the 3–electrode design has three major benefits. First, the energy of the main discharge now has minimal shot–to–shot variation decreasing the likelihood of carbonization on the propellant face. This should also have the effect of the MicroPPT delivering a more uniform impulse–bit if it were to be used in a mission requiring single shot operation. Second, the seed ionization from the trigger discharge greatly reduces the voltage required on the main discharge. For example, for a ¼" diameter outer electrode in a 2–electrode configuration, up to 40 kV is required to reliably initiate the discharge. With the 3–electrode design this voltage is typically 3 kV. This significant reduction in voltage greatly reduces the design requirements for the PPU. Third, the design is far more robust to short–term increases

Figure 4: Propellant carbonization decreases as capacitor energy rises.

in the voltage required to initiate the trigger discharge.

Firing frequency, or power level, in the 3–electrode design can be increased by decreasing the resistance in the trigger circuit, or by increasing the output current of the PPU.

The dimensions of the Teflon™ annuli in the 3–electrode design must still be correctly sized for their respective discharge energies to prevent carbonization. The determination of the required operating energy for a given propellant diameter is generally accomplished empirically, which is far faster and more accurate than trying to use modeling and simulation. An example is shown in Figure 4 where the carbonization pattern is shown for a ¼" propellant diameter at three different discharge energy levels after continuous firing for at least eight hours and at 1 Hz. These experiments were conducted in a glass bell jar at AFRL under a pressure of 10^{-6} Torr. The cases with higher discharge energy were fired for longer duration to see if carbonization needed longer time to appear. For these tests a ¼" diameter, 2–electrode MicroPPT test bed was energized using a 0.417 μF capacitor. The charge voltage ranged from 2448V for the 1.25 J case, to 5364V for the 6 J case. Clearly these voltages are insufficient to cause the surface breakdown needed for MicroPPT discharge initiation across a ¼" diameter. Rather than complicate the test setup by using the 3–electrode MicroPPT configuration, an auxiliary 0.5 J sparkplug was placed near the MicroPPT to initiate the discharge on command. It is apparent in the post–firing photographs of Figure 4 that the degree of carbonization decreases with increased discharge energy. Although two of the photographs in Figure 4 show very little axial recession, longer-duration tests with several inches of recession into the anode shell provided consistent results, The propellant rod must be disassembled in these tests to confirm that the propellant face is still free of carbonization. For the ¼" diameter propellant and the center electrode used in these tests, a 6–J discharge energy was found

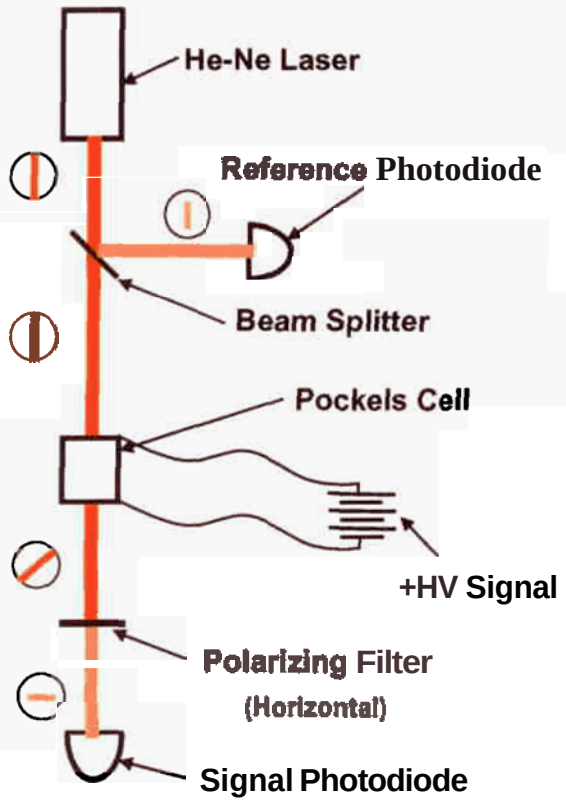

Figure 5: Pockels Cell voltage measurement schematic

sufficient for long–term operation. Once the Teflon™ annuli dimensions are matched to the design discharge energy, the center and intermediate electrode materials and thickness are adjusted to achieve relatively uniform recession of all components within the outer electrode.

MicroPPT Testing

Pockels Cell Voltage Measurements

The MicroPPT poses a unique dilemma for common voltage measurement techniques. Due to the high impedance present in the MicroPPT circuit, conventional high–voltage diagnostics are intrusive and cannot be used. In response to this need, development of a Pockels Cell voltage measurement is ongoing at AFRL.

A Pockels Cell rotates light polarization in proportion to an applied electric field. A polarized laser is directed through the Cell, rotating the beam polarization as shown in Figure 5. A polarized filter attenuates the beam and the intensity is measured by photodiodes before and after the Pockels Cell and filter combination. The ratio of the beam intensities

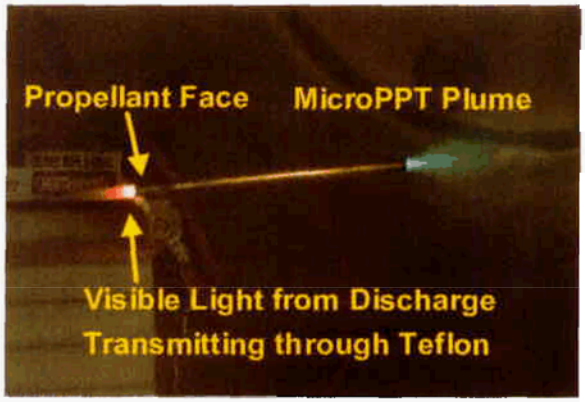

Figure 6: The 3–Electrode MicroPPT fires until all Teflon™ propellant utilized

is a precise and repeatable function of the applied voltage. Since the Pockels Cell draws no current, the infinite impedance assures a non–intrusive measurement of capacitor voltage for the MicroPPT.

Long–term Functionality and Lifetime

Once a MicroPPT design has demonstrated operability, the development effort shifts to demonstrating long–term reliability. The relative simplicity of the design lends itself to the simplest form of lifetime testing. A complete MicroPPT system of PPU, capacitors, and propellant module is assembled, placed within a vacuum chamber, and fired continuously until it fails or expends all of its available propellant. Testing focused on empirically optimizing the MicroPPT in terms of discharge energy, voltage, geometry, and electrode materials. The end result of this process is a baseline design that has exhibited a high degree of reliability.

A total of 12 long–duration tests have been performed on the MicroPPT baseline design. Of these 12 tests, two failed within a few hours and the remaining 10 operated successfully for over 100 hours until the propellant was expended. The two failures were attributed to propellant fabrication errors. Such failures are not a significant concern since they will be discovered during short– duration functionality testing prior to flight hardware delivery. Furthermore, since they are attributable to propellant fabrication, the failure rate should decrease as the fabrication procedures are refined.

In Figure 6, the propellant has receded within the anode tube about 6” until it resides slightly to the right of the end of the anode tube, as marked in the photograph. The blue MicroPPT plume is still visible at the exit plane of the thruster on the right. The

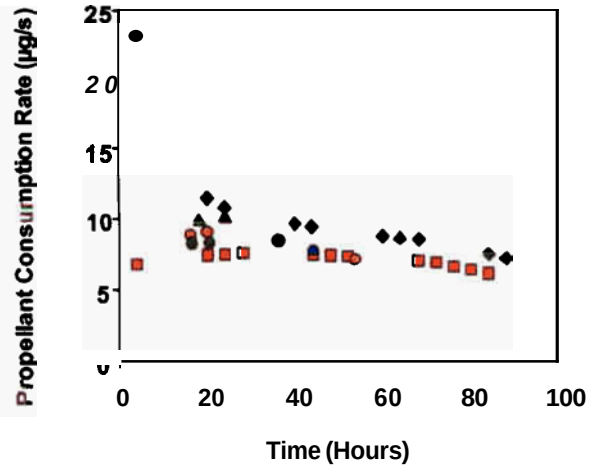

Figure 7: Propellant consumption over long–duration firings

orange visible emission on the left side of the anode tube is light from the discharge arc that is transmitting through the short region of the remaining solid propellant. Shortly after the photo in Figure 6 was acquired the Teflon™ propellant receded past the left edge of the anode tube, and the thruster failed due to a full expenditure of propellant.

Propellant Consumption Rate

Once long–term functionality had been established, tests were performed to investigate the potential for changes in the MicroPPT operation over time. The key issues in this regard are thrust and propellant consumption rate. The lack of good thrust data is discussed in a later section. Propellant consumption rate over long duration firings is shown in Figure 7. For these tests, the 3–electrode MicroPPT was fired at 2.25 J for at least four hours with a firing frequency of 1.0 ± 0.1 Hz. The thruster was then removed from the vacuum chamber, allowed to cool, weighed, and placed back in the vacuum chamber for continued firing. Tests in this manner were conducted on 5 different samples and extended up to 90 hours. Apart from an initial transient period, the propellant consumption rate is relatively constant for all of the samples until the propellant is fully expended. This observation supports the conclusion that long–term functionality has been achieved in the MicroPPT.

The propellant consumption rate in the current design of the MicroPPT raises two concerns. First, during the first four hours of testing, one sample is observed to have a propellant consumption rate three times higher than the average rate. This initial high rate could be attributed to improper propellant fabrication, improper propellant conditioning prior to the test, or an error in the experimental procedure. Ongoing tests at AFRL, which continue to add to the database of Figure 5, will be valuable in isolating the cause of the observed transient phase in the single test.

A second concern from the tests is that the propellant consumption rate is generally higher than that observed in breech–fed PPTs. The average rate is 8.6 µg/s with a standard deviation of 1.3 µg/s. By comparison, the propellant consumption rate for the breech–fed LES 8/9 was 28 µg/s for a 20 J, 1 Hz discharge. Using a linear scaling with energy and power, the propellant consumption rate for the MicroPPT is 2.7 times higher than that of LES 8/9.

One contributing cause is in the experimental procedure used to measure the propellant consumption. In previous PPT designs, the solid block of Teflon™ was simply removed, weighed, and reinstalled. In the MicroPPT this is impossible since the Teflonm propellant is tightly integrated with the electrodes. The Teflonm cannot be removed without causing permanent damage to the propellant module. Therefore, when the propellant consumption is measured for a MicroPPT, the measurement necessarily includes the mass loss of the electrodes. The mass fraction in the propellant module for the intermediate and center electrodes (ignoring the outer electrode since it largely survives) is 24.5%. If this mass is not counted in the propellant consumption rate, the average rate falls to 6.6 µg/s, which is still 2.1 times that expected by a linear scaling to the propellant consumption rate measured on the LES 8/9 PPT. It should also be noted that the electrode mass should not necessarily be excluded when considering the thruster specific impulse. This electrode material participates in the discharge and is likely accelerated to some degree along with the Teflon™ propellant. Electrode mass is also ablated and accelerated along with the Teflonm propellant in traditional PPTs, but the mass fraction of the metal in the effluent is negligible.

The somewhat high propellant consumption rate will be investigated as part of the on-going engineering development. However, it is also important to note that the measured rate is not grossly different than that measured on similar devices. For example, the coaxial gasdynamic PPT developed by Burton had an average propellant consumption rate of 40 µg/s for a 10 J, 1 Hz discharge.' This rate is slightly higher than that observed in the MicroPPT, and 2.9 times that measured on the LES 8/9 PPT.

Thermal Testing

Previous PPT research has shown that the propellant consumption rate in these devices has a small, but important, temperature dependence.[1] In a standard PPT under laboratory testing, variations in the propellant consumption rate are relatively small simply because the thermal mass of the device restricts the temperature variations to a small range. As the MicroPPT is miniaturized disproportionate to the decrease in operating power level, the relative thermal mass will decrease. This can result in larger propellant temperature increases when firing the MicroPPT, as compared to the standard PPT. These temperature increases may be a contributing source to the comparatively high propellant consumption rate that was observed for the MicroPPT.

In order to characterize temperature effects on the MicroPPT operation, temperature measurements were collected at locations along the outer electrode during normal operation. Three T–Type thermocouples were affixed to the copper outer electrode at the tip, at the center, and at the rear using Omega CC high–temperature cement. A photograph of the MicroPPT with the thermocouples attached is shown in Figure 8. Two different vacuum facilities were used for these measurements. The first is a glass bell jar set up to allow the entire thruster, including PPU, to fire in vacuum on a thermally isolated stand. The second facility is a steel bell jar where the MicroPPT entered the chamber clamped in a steel feed through. In this second facility, the steel feed through provided a thermal path to cool the MicroPPT outer electrode. The MicroPPTs were fired continuously at 2.25 J, 1 Hz for three days, during which time the Teflon™ propellant receded the entire length of the outer electrode.

Data from the thermally isolated experiment in the glass bell jar is shown in Figure 9. Data were not acquired during the first 4 hours of operation due to a temporary failure of the data acquisition system. During the first 4 hours, the temperature at all axial points along the outer electrode rises from 22°C to between 50°C and 65°C, depending on the axial location. Measurements near the tip, and the starting location of the discharge arc, initially show the highest temperature. The progression of the arc down the thruster tube is evident during the experiment as the tip is observed to cool, while the temperature measurement at the rear of the outer electrode is observed to rise. The MicroPPT reached a peak temperature at the tip of 65°C. Data from the experiment in the steel bell jar, which also included a

Figure 8: Cemented thermocouple placement on a MicroPPT tube

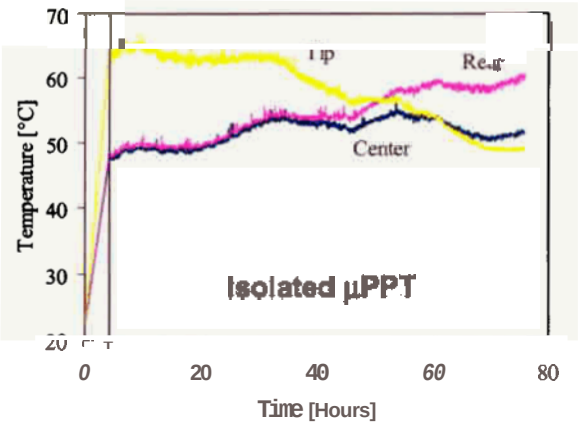

Figure 9: Temperature rise for a thermally–isolated MicroPPT

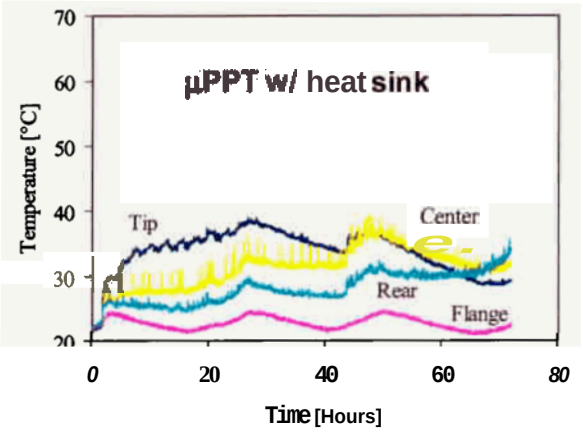

Figure 10: Temperature rise for a MicroPPT heat–sunk by clamping to a steel flange

Type–T thermocouple on the flange, are shown in Figure 10. The peak temperature is 25°C lower than the thermally isolated experiment, due to heat transfer to the flange. Fluctuations of the ambient temperature are observed on the flange and, to a lesser degree, are transmitted to the thruster itself, indicating that the thermal path provided by the flange is indeed affecting the temperature of the MicroPPT. These tests suggest that significant

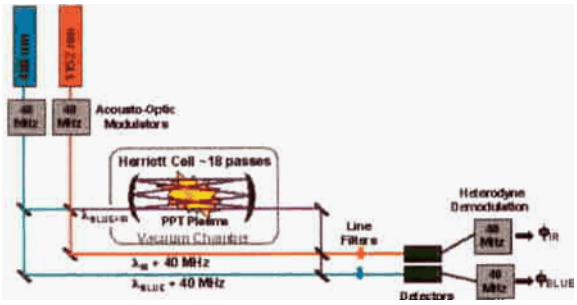

Figure 11: Interferometer Layout

control can be gained over the MicroPPT temperature through proper design of the thermal paths. This is not true in a standard PPT where the larger propellant dimensions and low thermal conductivity of Teflon™, lead to the propellant itself acting as a large thermal mass. Attempts at AFRL to significantly control the Teflon™ propellant temperature in a standard PPT through modifications to thermal path were largely unsuccessful.

The importance of the temperature effects is not yet certain. At the nominal operating power of 2.25 W it may be that the temperature increase is insufficient to cause a significant increase in the propellant consumption rate. Propellant consumption tests are now being performed for the case where the thruster is thermally isolated in the glass bell jar. It is also important to note that the MicroPPT power may be raised, which could make the temperature effect on propellant consumption more important.

MicroPPT Plasma Diagnostics

The small plasma volume generated by the MicroPPT creates a significant diagnostic challenge. For material probes, such as electrostatic or magnetic field probes, the characteristic length of the probe is comparable to or larger then the MicroPPT plasma volume.'' For interferometric techniques to measure density, the measurement resolution is constrained by the short scale length of the plasma.[7] Since the interferometer measures a phase shift proportional to the product of the density and the laser path length through the plasma, the fundamentally short path length results in excessive measurement uncertainty for the line–averaged plasma density.

To address this problem, a Hemott Cell'' interferometer was used and a techni ue employing a 'point measurement' was developed.' This technique converges multiple laser passes in a Heniott Cell down to a small area, thereby providing increased laser path length within the plasma. By focusing a large number of laser beams into a small measurement volume, the Hemott Cell increases the instrument resolution by a factor of about 10, compared to a single–pass interferometer, with minimal degradation of spatial resolution. Electron density is measured with a single–wavelength Herriott cell and compared with numerical predictions. Efforts to measure the neutral density after the current pulse using a 2nd laser frequency are discussed in a previous work.[14]

Previous modeling efforts have indicated that the plasma distribution in the plume field heavily depends upon upstream boundary conditions.[6,15,16] Therefore the model of the plasma generation in these devices becomes a very important aspect of accurate plasma plume simulation. Inspection of the Micro–PPT propellant surface after firing indicated signs of charring and preferential ablation near the electrodes.[17,18] In this paper we present results of the microscopic analyses of the charred areas and propose a mechanism of the char formation. In order to understand this phenomenon, a model of the plasma layer near the Teflon'''' surface is developed. In addition, the solution of the model provides boundary conditions for simulating the plasma plume.[6]

Herriott Cell Measurements

The MicroPPT testbed for the Herriott Cell measurements uses a coaxial geometry, shown in Figure 1, with bare copper outer anode and central cathode that is silver-coated copper. The outer diameter of the thrusters tested here is 6.35 mm while the outer Teflon™ diameter is 5.46 mm. The cathode diameter is 1.64 mm. A DC–DC converter charges a 0.417 μF capacitor to 5.6 kV, corresponding to a stored energy of 6.6 J. Not shown in Figure 1 is the external sparkplug used to initiate the discharge in the testbed configuration. A 0.5'' diameter plug is placed approximately 2 cm from the propellant face, at a 45–degree angle, and discharged with a 0.5 J capacitor that is triggered from the data acquisition system.

Interferometer Layout

The interferometer employs quadrature heterodyning technique and a Herriott Cell for increased path length exposure. Detailed descriptions of these are given elsewhere.[7,14,19] Figure 11 gives a general layout of the interferometer with the optional second laser frequency.

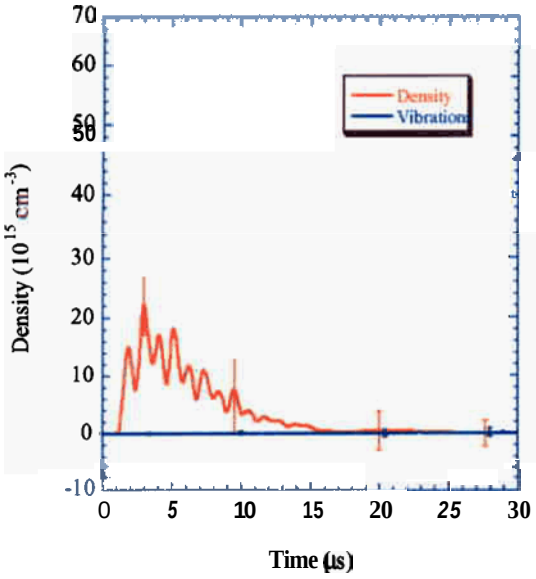

Figure 12: Electron density with vibrations for 13–pass Herriott Cell. 5 mm from fuel face and 6.6 J.

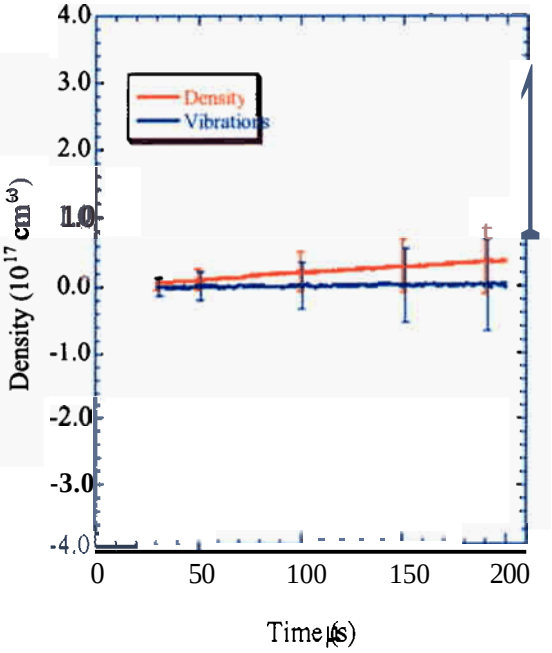

Figure 13: Neutral density measurements from 13 pass Herriott Cell interferometry. Data taken at 5 mm from fuel face for 6.6 J discharge.

A Bragg cell splits the 150 mW Argon–ion laser (488 nm) into scene and reference beams using a 40 MHz shift in the reference beam. The scene beam is directed into the vacuum tank through a viewport and into the Hemott Cell optics. The Hemott Cell optics for the point measurement configuration require the Hemott Cell mirrors as well as focusing and guiding optics for the input and exit beams. The MicroPPT is situated halfway between the Herriott Cell mirrors.

The scene beam is returned to the external optics table and recombined with the reference beam that travels the same path length. The combined beams are focused on the detector for optimal measurement intensity.

Two–Color Interferometer

A two-color interferometer was also constructed for baseline comparison of electron and neutral densities. This interferometer allows separation of electron and neutral densities throughout the pulse. A 488–nm Ar–ion laser was used simultaneously with an 1152–nm HeNe laser providing direct measurements of both electron and neutral densities early in the pulse. This data is taken at 5–mm distance from the fuel face and provides the control case for density measurements with the Hemott Cell.

Density Measurements

The data from the two–color interferometer shows electron and neutral density at 5 mm from the fuel face for 6.6 J discharge and 13 passes. Figure 12 shows this data for the first 30 μs after the discharge. Peak electron density reaches $2.1 \pm 0.3 \times 10^{16}$ cm^{-3}.

Over a large number of discharges, uncertainty introduced by vibration effects and shot–to–shot thruster variation overwhelms the neutral density signal disallowing a definitive measurement. For a single discharge, the neutral density is typically resolved. Figure 13 shows neutral density data with typical error bars taken at 5 mm from the fuel face using the 13–pass Hemott Cell. The data indicate that at 200 μs after the discharge, neutral density is no larger than 8.5×10^{16} cm^{-3}.

Thruster and Model Comparisons

A significant finding of this experiment is the degree of agreement between theoretical modeling predictions and experimental results. A figure of merit is required to compare and contrast systems that are not similar in energy or dimension. The energy–to–area ratio provides such a basis and is used here to investigate the comparison between past and current predictions and measurements.

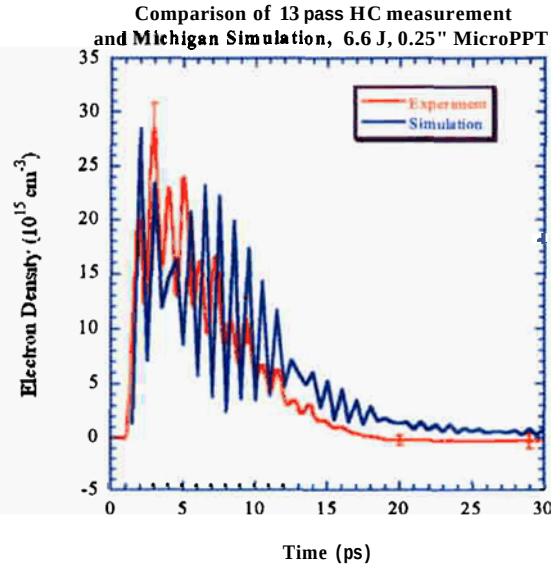

Figure 14: Comparison of predicted and measured electron density time variation at 5 mm from the propellant face at the axis in the case of 6.35–mm diameter MicroPPT firing at 6.6 J.

A hybrid fluid–PIC–DSMC approach is used to predict electron density.[6] The energy–to–area ratio for this model is higher than that of the experimental setup used. This is balanced by increased electron density.

Predictions made for the 6.35–mm diameter MicroPPT show strong agreement with experimental data. Description of the model is given elsewhere.[7,12] Figure 14 shows direct comparison of predicted electron density using an experimental current waveform as input. The red line shows density measured using the Hemott Cell. The degree of agreement is apparent, and provides support for the model being developed.

External Electron Density

Hemott cell measurements give strong evidence of plasma presence as much as 3 mm behind the exit plane. A MicroPPT ablation model presented elsewhere predicts non–zero carbon ion densities at the exit outside a 3.1 mm diameter MicroPPT.[6] Plasma backflow and external arc attachment can explain this phenomenon.

Plume Imaging

In order to better understand the potential for spacecraft integration, further validate the plume model, and help the designers determine the optimal MicroPPT placement on the spacecraft, a series of tests were conducted to characterize the MicroPPT plume divergence. For this study, a ¼" diameter, 2–electrode MicroPPT was energized to 5 J and triggered by an external spark ignitor. The tests were conducted in a vacuum chamber pumped down to 2 x 10^{-5} Torr. The plume emission was collected using an intensified CCD array (Cooke DiCam) with nanosecond framing capability and peak spectral response in the visible portion of the spectrum. The goal of the test was to characterize the plume divergence for both the initial plasma exhaust and for the late time vaporization (LTV). The LTV consists of neutrals and particles emitted from PPTs for a few milliseconds after the current discharge and plasma has extinguished.[20] Estimates indicate that LTV contains as much as 90% of the expended propellant mass so it is critical to consider this component of the exhaust when considering spacecraft interaction. Plume divergence measurements are collected for the MicroPPT at beginning-of–life (BOL) when the propellant face is at the exit plane of the thruster, and after significant recession has occurred.

The intensity, general shape and size of the observed MicroPPT plume was uniform and repeatable at all propellant depths. LTV images, by their very nature, are erratic from shot–to–shot as they capture trails of individual particles exiting from the thruster rather than a uniform, expanding plasma. Despite this irreproducibility, the overall divergence of the LTV was repeatable at all depths. Figure 15 shows the MicroPPT plume at BOL, and at a fuel depth of 30 mm. The plasma plume is initially well–directed with virtually no divergence, a characteristic common at all depths. Further into the flow field, the plasma diffuses into a 60°–70° cone. The CCD gain was held constant for the tests, resulting in decreased brightness for the recessed plasma and neutral/particulate plumes. At BOL, the MicroPPT is seen to emit particulates into the entire 180" plane at the thruster tip. As the propellant face is recessed into the outer electrode, a dramatic decrease in the LTA divergence angle is observed. The measured divergence angle, as a function of the recession depth of the propellant is shown in Figure 16 for both the plasma and LTV (neutrals/particles) emission. The images of Figure 15 and the plot of Figure 16 suggest that intentionally recessing the propellant face at beginning of life may significantly reduce the

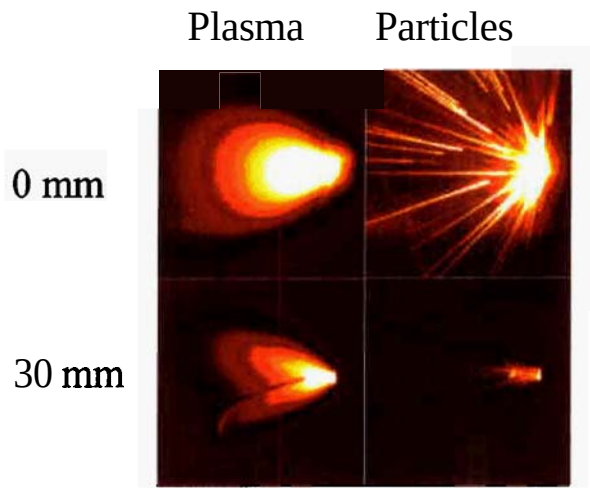

Figure 15: Plasma and Late Time Vaporization divergence in a ¼"–diameter, 2–electrode MicroPPT firing at 5 J. The curved rod visible in the plasma pictures is an spark plug used to ignite the main discharge.

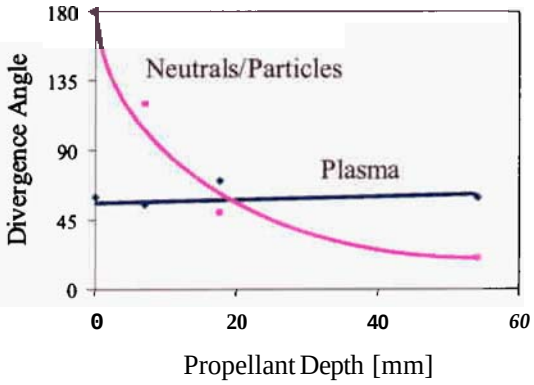

Figure 16: The divergences of the plasma and LTV effluents. The area affected by potentially contaminating particulates greatly reduces as propellant recesses.

potential for spacecraft contamination from the neutrals and particles.

Summary

A miniaturized version of the PPT, a MicroPPT, has been developed at AFRL for use as primary propulsion on 25–kg-class spacecraft and secondary propulsion/ACS on 100–kg class spacecraft. A 3–electrode configuration has been implemented which removes nearly all of the legacy technology from the LES 8/9 PPT, including the spark plug and ignitor circuitry. The MicroPPT circuit provides a robust mechanism for initiating the discharge across the Teflon™ face.

A Pockels Cell has been developed and is in use as an alternative voltage diagnostic for MicroPPTs. This has been shown to allow voltage measurements in cases where the typical voltmeter impedance is too large to produce a reliable measurement.

Life tests have shown high reliability with thruster failures only occurring shortly into the testing cycle due to thruster fabrication errors. Performance tests, hampered by electronics failures on the thrust stand, are on–going. These will be followed by flight design, fabrication, and environmental tests.

Thermocouple tests indicate that providing a thermal path from the thruster to a heat sink can significantly reduce temperatures in the MicroPPT tube. Tests will be performed to indicate whether the lower temperatures will correspond to lower ablation rates.

An examination of the plume of a MicroPPT utilizing a dual–wavelength and a 13–pass Hemott Cell system indicates a peak electron density $n_e = 2.1 \pm 0.3 \times 10^{16}$ cm^{-3}. Attempts to measure neutral density with the increased resolution of the interferometer were unsuccessful. For standard PPTs, the Hemott Cell has been effective in measuring neutrals as late as 200 µs after the pulse for single shots, with averaged neutral density measured out to 150 µs.[13] However, previous measurements used the Hemott Cell without external focusing optics and were therefore less susceptible to mechanical vibrations late in time. Past measurements also used higher numbers of passes in the Hemott Cell that are not achieved here. The neutral density is bracketed by an upper limit $n_n = 8.5 \times 10^{16}$ cm^{-3} at 200 µs after the pulse is established.

Agreement between present electron density measurements and numerical predictions is strong. Comparison by the energy–to–area ratio argument for the 3.1–mm MicroPPT matches well using curve–fit data taken here. Also, specific predictions using the current waveform as an input followed measured electron densities very closely. This indicates some level of validation for the numerical model.

Spacecraft interaction tests indicate that the plasma plume shape can be well–characterized and accounted for in spacecraft integration. The divergence of the late time vaporization, which

evolves after the plasma, is strongly linked to the recession of the Teflon™ in the MicroPPT. An initial recessing of the fuel at BOL may be necessary to reduce solid Teflon™ deposition on spacecraft surfaces

Acknowledgements

The authors acknowledge the excellent technical support of Paul Adkinson of Sverdrup Technologies and Emily Blundell and Garrett Reed of W. E. Research.

References

[1] Spanjers, Gregory G., "Micro Pulsed Plasma Thruster having Coaxial Cable Segment Propellant Modules," Patent Number US 6,269,629 awarded Aug 7,2001.

[2] McGuire, M. L. and Myers, R.M., "Pulsed Plasma Thrusters for Small Spacecraft Attitude Control," GSFC Flight Mechanics/Estimation Theory Symposium, May 13–16,1996.

[3] Burton, R.L., and Turchi, P.J., "Pulsed Plasma Thruster," Journal of Propulsion and Power, Vol. 14, No. 5, 1998.

[4] Spanjers, Gregory G., "Self–Triggering Micro Pulsed Plasma Thruster," Provisional US Patent 09/518,164, March 6,2000.

[5] Gulczinski III, F. S., Dulligan, M. J., Lake, J. P., Spanjers, G. G., "Micropropulsion Research at AFRL," 36" Joint Propulsion Conference, AIAA Paper 00–3255, July 2000.

[6] Keidar, M. and Boyd, I.D., "Electromagnetic Effects in the Near Field Plume Exhaust of a Pulsed Plasma Thruster," AIAA Paper 2001–3638, July 2001.

[7] Spanjers, G. G., McFall, K. A., Gulczinski, F. S., and Spores, R. A., "Investigation of Propellant Inefficiencies in a Pulsed Plasma Thruster," 32nd Joint Propulsion Conference, AIAA Paper 96–2723, July 1996.

[8] Spanjers, Gregory G., Schilling, John, and White, David, "Methods to Increase Propellant Throughput in a Micro Pulsed Plasma Thruster," US Provisional Patent filed July 2001.

[9] Burton, R. L. and Bushman, S. S., "Probe Measurements in a Coaxial Gasdynamic PPT," 35" Joint Propulsion Conference, AIAA Paper 99–2288, June, 1999.

[10] Spanjers, G. G., Malak, J. B., Leiweke, R. J., and Spores, R. A., "The Effect of Propellant Temperature on Efficiency in a Pulsed Plasma Thruster," Journal of Propulsion and Power, Vol. 14, No. 4, July–August 1998.

[11] Spanjers, G.G. and Spores, R.A., "PPT Research at AFRL: Material Probes to Measure the Magnetic Field Distribution in a Pulsed Plasma Thruster," 34" AIAA Joint Propulsion Conference, AIAA Paper 98–3659, Cleveland, OH, July 12–15,1998.

[12] Hemott, D.R., Kogelnik, H., Komfner, R., "Off Axis Paths in Spherical Mirror Interferometers," Applied Optics, 3,1964,523.

[13] Antonsen, E.L., Burton, R.L., Engelman, S.F., Spanjers, G.G., "Hemott Cell Interferometry for Unsteady Density Measurements in Small Scale Length Thruster Plasmas," AIAA Paper 2000–3431, July 2000.

[14] Antonsen, E. L., "Hemott Cell Interferometry for Pulsed Plasma Density Measurements," MS Thesis, University of Illinois at Urbana-Champaign, 2001.

[15] Boyd, I. D., Keidar, M., and McKeon, W., "Modeling of a Pulsed Plasma Thruster from Plasma Generation to Plume Far Field," Journal of Spacecraft and Rockets, Vol. 37, No. 3,2000, pp. 399–407

[16] Keidar, M. and Boyd, I.D., "Device and Plume Model of an Electrothermal Pulsed Plasma Thruster," AIAA Paper 2000–3430, July 2000.

[17] White, D., et al., "AFRL MicroPPT Development for Small Spacecraft Propulsion," 33rd AIAA Plasmadynamics and Lasers Conference, AIAA Paper 2002-2120, Maui, HI, May 2002.

[18] Keidar, M., Fan, J., Boyd, I.D., and Beilis, I. I., "Vaporization of Heated Materials Into Discharge Plasmas," Journal of Applied Physics, 89,2001, pp. 3095–3098.

[19] Antonsen, E. L., "Hemott Cell Interferometry for Pulsed Plasma Density Measurements," MS

Thesis, University of Illinois at Urbana-Champaign, 2001.

[20] Spanjers, G. G., Lotspeich, J. A., McFall, K. A., Spores, R. A., "Propellant inefficiency resulting from particulate emission in a Pulsed Plasma Thruster," Journal of Propulsion and Power, Vol. 14, No. 3, May–June 1998.